Polymer 53 (2012) 2412–2421

Contents lists available at SciVerse ScienceDirect

Polymer

journal homepage: www.elsevier.com/locate/polymer

Nano- and microstructural effects on thermal properties of poly (L-lactide)/multi-wall carbon nanotube composites

E. Lizundia [a,*], A. Oleaga [b], A. Salazar [b], J.R. Sarasua [a,*]

[a] Department of Mining–Metallurgy and Materials Science, School of Engineering, University of the Basque Country (EHU-UPV), Alameda de Urquijo s/n, 48013 Bilbao, Spain
[b] Applied Physics Department, School of Engineering, University of the Basque Country (EHU-UPV), Alameda de Urquijo s/n, 48013 Bilbao, Spain

ARTICLE INFO

Article history:
Received 22 December 2011
Received in revised form
26 March 2012
Accepted 27 March 2012
Available online 2 April 2012

Keywords:
Poly (L-lactide)
Carbon nanotube (CNT)
Interfacial thermal resistance

ABSTRACT

In this work the thermal properties of poly (L-lactide)/multi-wall carbon nanotube (PLLA/MWCNT) composites have been investigated. Thermal conductivity was determined after measuring specific heat capacity (C_p), thermal diffusivity (D) and bulk density (ρ) of composites. Thermal conductivity rises up to 0.345 W/m K at 5 wt.% after reaching a minimum value of about 0.12 W/m K at 0.75 wt.%. In order to understand the heat-conduction process, experimentally obtained thermal conductivities were fitted to an existing theoretical model. The much lower thermal conductivity of composites compared with the value estimated from the intrinsic thermal conductivity of the nanotubes and their volume fraction could be explained in terms of the obtained large thermal resistance (R_k) of $1.8 \pm 0.3 \times 10^{-8}$ m^2 K/W at nanotube–matrix interface. The CNT dispersion in the composites was analyzed by atomic force microscopy (AFM) and transmission electron microscopy (TEM). Although the thermal resistance dramatically reduces the estimated bulk thermal conductivity of composites, the existence of an interconnected conductive nanotube network for thermal diffusion in PLLA/MWCNT composites demonstrates that the addition of carbon nanotubes represents an efficient strategy in order to successfully enhance the thermal conductivity of insulator polymers.

1. Introduction

Since the discovery by Iijima in 1991 [1,2] carbon nanotubes (CNT) are being widely investigated for composite applications. Nowadays, the development of conductive nanofiller-based composites has become an attractive new research area in material science. For instance, even with very low contents of conductive carbon nanotube loadings polymer composites present usually a valuable jump in electrical conductivity with regard to the insulating matrix. As a matter of fact electrical percolation effects have been found in many polymer/CNT nanocomposites [3–7] with percolation thresholds achieved at low concentrations ranging from 0.0025 wt.% to 7 wt.%, exhibiting electrical conductivities of about 1×10^{-4}–1×10^{-1} S/m (for percolated compositions) that make possible the use of polymer matrix composites (PMC) in conductive applications.

On the opposite, although several works have tried to demonstrate it [8–10], thermal percolation in polymer composites is not well defined and remains as a dubious subject open to debate. Phonons are the primary mode of heat conduction of carbon nanotubes [11,12] leading to extremely high thermal conductivity (due to their graphitic structure), with published experimental values [13,14] between 1750 and 3000 W m^{-1} K^{-1} and a simulated theoretical values of 6600 W m^{-1} K^{-1} [15]. As occurs with electrical conductivity, in composites of thermally insulating polymer matrices with well-dispersed conductive carbon nanotubes the thermal conductivity should also increase at low critical concentrations [16,17]. In this hypothesis, obvious nanotube applications would open through the development of thermally conductive polymer-based composites, for example to be used as heat dissipation or thermal interface materials, actuators [18], electromagnetic interference (EMI) shielding [19], solar cells [20], etc. It is reported that composites with a thermal conductivity from 1 to 30 W/m K are required for some applications such as heat sinks in electric or electronic systems [21].

However, although several approaches have been taken into account in order to improve the thermal conductivity of polymers, the experimental values of polymer/CNT composites show that thermal conductivity is not increased as expected, yielding thermally low conductive materials with increasing thermal conductivity in regard to neat polymer from 0.3 W m^{-1} K^{-1} to

* Corresponding authors. Tel.: +34 94 601 4271; fax: +34 94 601 3930.
E-mail addresses: erlantz.liizundia@ehu.es (E. Lizundia), alberto.oleaga@ehu.es (A. Oleaga), agustin.salazar@ehu.es (A. Salazar), jr.sarasua@ehu.es (J.R. Sarasua).

0032-3861/$ – see front matter © 2012 Elsevier Ltd. All rights reserved.
doi:10.1016/j.polymer.2012.03.046

0.7 W m^{-1} K^{-1} at 17 wt.% loading for PEEK/MWCNT system [22] from 0.156 W m^{-1} K^{-1} to 0.158 W m^{-1} K^{-1} at 0.7 vol.% for PVC/MWCNT composite [23] from 0.18 W m^{-1} K^{-1} to 0.45 W m^{-1} K^{-1} at 9 vol.% for PMMA/SWCNT system [24] or from 0.233 W m^{-1} K^{-1} to 0.537 W m^{-1} K^{-1} at 49 vol.% loading for PVDF/SWCNT composites [25]. This may be due to the presence of an interfacial thermal resistance between carbon nanotubes and the polymer matrix, which is known as Kapitza resistance [26]. This resistance occurs when the thermal conductivity of matrix differs a lot from the inclusion's thermal conductivity, increasing the resistance with the mismatch [27–29]. Due to the large specific surface area of carbon nanotubes, the existence of this thermal boundary resistance can dramatically reduce thermal conductivity of MWCNT composites in regard to single MWCNT [30]. Therefore, one of the main goals in thermally conductive polymer/CNT composites will be the development of composite materials with low thermal interface resistances.

In order to interpret the effective thermal conductivity in the case of nanotube composites an effective medium approach (EMA) can be applied [31]. This physical model describes the macroscopic property of a medium based on the properties and the relative fractions of its components. According to the model developed by Nan et al. [32], the thermal conductivity values of both matrix and nanotubes, the dimensions of the individual rods, as well as the interfacial resistance at the nanotubes/matrix interface must be taken into account.

Among all the biopolymers, poly (L-lactide) (PLLA) is of special interest. Up to now, this polymer has been basically used in biomedical [33] and biodegradable packaging [34] applications. However, recent progress in production of PLLA at low cost is accelerating its use as a commodity plastic [34]. With the addition of carbon nanotubes the thermal conductivity of PLLA can be enhanced, making this material suitable for general purpose plastics, being environmentally friendly materials with diverse industrial uses [35,36]. The synergetic effect obtained from combination of biodegradable polymers and carbon nanotubes opens new insights in the potential applications of PLLA for regenerative medicine applications [7,37].

In this way, the aim of this work is to characterize the thermal properties of these composites in order to evaluate the improvement of heat transport at certain compositions, which will have a direct influence on their technical applications (thermally conductive nanocomposites would replace the need of heavy metallic components that are used for cooling of electronic circuits and propulsion systems [38]). A particular goal is to explore the possibilities of an important increase of the thermal conductivity as compared to the electrical percolation phenomena well known in these materials.

In this work we attempt to correlate the thermal and morphological properties of PLLA-based composites prepared by a melt mixing process. In this way, modulated differential scanning calorimetry (MDSC), high-resolution ac photopyroelectric calorimeter, dynamic light scattering (DLS), atomic force microscopy (AFM) and transmission electron microscopy (TEM) techniques were used. The continuous development of a thermally conducting pathway within composites with further addition of carbon nanotubes results in an enhancement of heat capacity, thermal diffusivity and thermal conductivity for concentrations larger than 1.25 wt.%, after reaching a minimum value at 0.75 wt.% loading. This behaviour is interpreted in terms of interfacial thermal resistance that reduces the expected thermal conductivity values of CNT-based composites when compared with the value estimated from the intrinsic properties of the nanotubes and their weight fraction. Obtained results assess the importance of using physically sensible models to interpret the thermal conductivity of these systems, stressing the role of the interfacial thermal resistance between the matrix and the nanotubes. This paper provides light on the understanding of thermal-conduction mechanism involved within polymer/CNT nanocomposites and gives insights about the next steps towards the complete understanding of thermal-conduction mechanism involved in polymer/CNT composites.

2. Experimental section

2.1. Materials

Poly (L-lactide) hereafter termed PLLA of number-average molecular weight (M_n) 153,000 g/mol and polydispersity index (M_w/M_n) 1.38, Biomer® (Germany) was used as matrix to prepare nanocomposites. The multi wall carbon nanotubes (MWCNT) were supplied by Arkema, grade Graphistrenght™ C100. Arkema uses a continuous synthesis process based on Catalytic Chemical Vapour Deposition (CCVD) in a fluidized bed type reactor, where nanotubes were grown on iron particles. The degree of purity of those nanotubes was 90 wt.%, with length ranging from 0.1 to 10 μm, outer mean diameter in the range of 10–15 nm, a mean number of walls of 10–15 [39].

2.2. Sample preparation

Prior to blending, PLLA pellets were dried in an air circulating oven at 40 °C and 8% of RH for 15 h, while the as-received MWCNT were dried at 120 °C and 8% of RH for 15 h. A composite system containing 0, 0.75, 1.25, 2.5, 4 and 5 wt.% MWCNT was prepared. The desired proportions of PLLA pellets with the carbon nanotubes were melt mixed in a Brabender Plasticorder PL2000 at 50 rpm. The temperature used was 200 °C and the mixing time 5 min. The blends obtained were conformed in sheets of 340 ± 15 μm thick in a hydraulic hot press by compression moulding at 200 °C under a pressure of 4 bar for the first 2 min and 240 bar for additional 3 min. Solidification was carried by water quenching. Once obtained the sheets were cut into discs with diameter of 6 mm, weighing around 12 mg.

2.3. Modulated differential scanning calorimetry (DSC)

The *Specific heat capacity* (C_p) of the composites was measured in a modulated differential scanning calorimeter MDSC of the Q200® series of TA Instrument Inc. Dry nitrogen was used as purge gas at a rate of 50 ml/min in all measurements. The measurements were conducted within a range comprised between −20 °C and 25 °C; below the glass transition temperature of PLLA, hence eventual recrystallization of PLLA during the scan was prevented. Temperature and enthalpy calibrations were performed using indium as standard. Heat capacity calibration was performed with a standard of sapphire (Al_2O_3, supplied by TA Instruments with a mass of 21.8 mg) within a range from −13.15 to 76.85 °C. C_p measurements were conducted in *heat only* MDSC mode with a modulating period (P) of 100 s, a temperature-oscillation amplitude of ±1.326 °C and a heating rate of 5 °C/min. In order to assure the reproducibility of the *Specific heat capacity* measurements of PLLA/MWCNT composites and erase any temperature gradient between the lower and upper part of samples, specimens of 340 ± 15 μm thick were analyzed. Reported heat capacity values correspond to the mean value over at least four measurements.

The crystalline fraction (X_c) % attributable to the non-isothermal PLLA crystallization during the rapid solidification by water quenching was determined by standard DSC as follows:

$$X_c(\%) = \frac{\Delta H_f - \Delta H_c}{\Delta H_f^0 \cdot W_m} \cdot 100 \quad (1)$$

where ΔH_f and ΔH_c are respectively the enthalpy of fusion and cold crystallization of the samples determined on the DSC and W_m is the PLLA matrix weight fraction in the composite sample. "Glass transition is a thermodynamic second order transition; i.e. there is a slope change in the first derivative magnitudes of free energy (such as specific volume or enthalpy) hence a change in heat capacity appears as a step in the baseline of the recorded DSC signal. In contrast, both crystallization and melting are first order transitions where a latent heat change occurs and the sample undergoes an abrupt volume change, resulting respectively as exothermic and endothermic peaks during the heating scan. The heat of fusion (ΔH_f) corresponds to the enthalpy change of the crystalline domains when they are melting, while the heat of cold crystallization (ΔH_c) is the enthalpy change associated to the development of partial crystallinity during the DSC heating scan". $\Delta H_f^0 = 106$ J/g was taken as the heat of fusion of an infinitely thick PLLA crystal [40,41].

2.4. Transmission electron microscopy (TEM)

The morphology and state of dispersion carbon nanotubes within the PLLA matrix were evaluated using a transmission electron microscope (TEM). Ultrathin sections of the nanocomposites (thickness of approx. 150 nm) were cut using a Leica Ultracut UCT (LKB Ultratome III) ultramicrotome equipped with a diamond knife. TEM was carried out using a Philips CM120 Biofilter apparatus with STEM module at an acceleration voltage of 120 kV. Images were acquired with a Morada digital camera.

2.5. Atomic force microscope (AFM)

Surface morphologies of PLLA and its composites were studied with a Veeco Instrument's MultiMode SPM 004-130-000 atomic force microscope at room temperature. The previously fabricated thick films were cut and adhered to an AFM mounting disk and melted at 210 °C in a convection oven for 3 min. Melted films were quenched in air at −10 °C; any further development of crystallinity was prevented. This way during the AFM analysis only the influence of carbon nanotube concentration can be analyzed without the interference of the presence of PLLA crystals.

The Veeco NanoScope V531r1 program was employed to analyze the recorded images. All experiments were carried out in contact mode. A Si_3N_4 cantilever (NP-10) with a characteristic force constant of approximately 0.58 N/m and a tip with radius of 10 nm was used to evaluate the dispersion of nanotubes. Resolution of 512 × 512 data points at 2 Hz per image was used to collect the images. In the discussion part only representative images of the samples will be shown.

In order to quantify the vertical deviation or the surface roughness of composites two parameters were employed. Root Mean Square Roughness is the standard deviation of the Z values within a given area and is calculated by the following equation:

$$R_q = \sqrt{\frac{\sum_{i=1}^{N} (Z_i - Z_{ave})^2}{N}} \quad (2)$$

where Z_{ave} is the average Z-value in the analyzed area, N is the number of points employed and Z_i is the current Z-value. The Mean Roughness (R_a) represents the arithmetic average of the deviation from the centre plane, determined by:

$$R_a = \frac{\sum_{i=1}^{N} |Z_i - Z_{cp}|}{N} \quad (3)$$

where Z_{cp} is the Z-value of the centre plane. Both R_q and R_a measurements represent the average vertical deviation of the surface profile from the centreline. Please note that these parameters can be appropriately used for seek of comparison, because all surfaces were generated by the same preparation method.

2.6. Thermal diffusivity measurements

The thermal diffusivity of PLLA and its composites was measured using a high-resolution ac photopyroelectric calorimeter in the standard back detection configuration [42]. A mechanically modulated He–Ne laser beam of 5 mW illuminates the upper surface of the sample under study. Its rear surface is in thermal contact with a 350 μm thick $LiTaO_3$ pyroelectric detector with Ni–Cr electrodes on both faces, by using an extremely thin layer of high heat-conductive silicone grease (Dow Corning, 340 Heat Sink Compound). The photopyroelectric signal is processed by a lock-in amplifier in the current mode. Both sample and detector are placed inside a nitrogen bath cryostat that allows measurements in the temperature range from 77 K to 500 K, at rates that vary between 100 m K/min and 1 m K/min according to the required resolution. If the sample is opaque and thermally thick (i.e. its thickness ℓ is higher than the thermal diffusion length ($\mu = \sqrt{D/\pi f}$) the natural logarithm and the phase of the normalized photopyroelectric current at a fixed temperature have a linear dependence on $\sqrt{f}$, with the same slope m, from which the thermal diffusivity of the sample can be measured [42].

$$D = \frac{\ell^2 \pi}{m^2} \quad (4)$$

In fact, the parallelism between both straight lines served as a test of consistence. It is worth mentioning that photopyroelectric calorimetry is a very precise technique to measure thermal transport properties, since small temperature gradients in the sample produce a good signal-to-noise ratio, letting thermal diffusivity be measured with high accuracy.

The thermal diffusivity of PLLA and its composites with several concentrations of MWCNT varying from 0.75 wt.% to 5 wt.% was measured. The thickness of all these plates was around 400–500 μm. The front surface of the plates was coated with a thin metallic layer (~1 μm) in order to fulfil the opaqueness condition.

2.7. Dynamic light scattering

Particle size analysis was performed on a Zetasizer Nano S from Malvern Instruments which covers a range from 0.6 nm to 6 μm. Each composition was dissolved at 2 wt.% (MWCNT respect to $CHCl_3$) in chloroform and stirred for 2 h at room temperature. In order to obtain fine-black suspensions, the resulting dissolutions of PLLA/MWCNT composites were further dispersed in chloroform in an ultrasonic bath (50 kHz, 100 W) for different times in a cold water bath. All the measurements were made at 20 °C in a glass cuvette with square aperture, being the carbon nanotube refractive index set to 2.42. Refractive index was set to be 1.446, while the viscosity of all dissolutions was set to be 0.38 cP.

3. Results and discussion

3.1. Differential scanning calorimetry (DSC) results

Fig. 1 presents the DSC traces of PLLA and PLLA/MWCNT composites after conformation by melt pressing and water

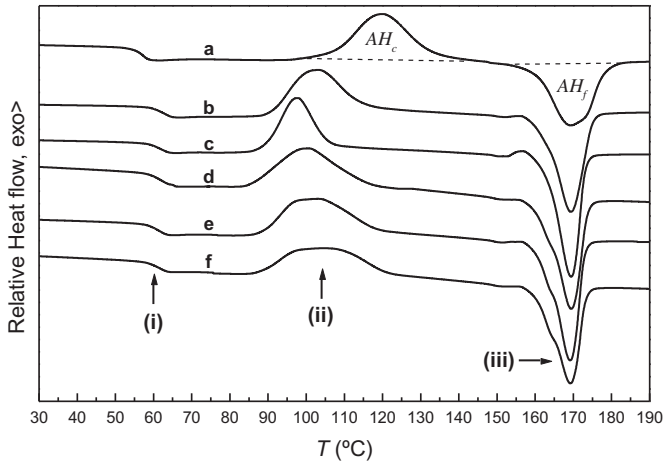

Fig. 1. DSC traces of water quenched PLLA/MWCNT composites at: (a) 0 wt.%, (b) 0.75 wt.%, (c) 1.25 wt.%, (d) 2.5 wt.%, (e) 4 wt.% and (f) 5 wt.%. In addition: (i) corresponds to the glass transition around 57–62 °C, (ii) corresponds to the cold crystallization peak and (iii) corresponds to the melting of PLLA between 160 and 180 °C.

quenching. As can be seen the glass transition temperature of neat PLLA appears at 56.6 °C, which is elevated by 5.3 °C for 0.75 wt.% MWCNT composite. It is also noted that larger amounts of nanotubes in composites do not affect the T_g position of PLLA that remains approximately constant at 62 °C. The T_g increase in PLLA composites in regard to neat PLLA can be associated to the confinement of PLLA chains by the many interfaces provided by the MWCNT themselves. On the other hand, the fact that the restrain to polymer chain mobility associated to the T_g increase in PLLA is not observed beyond 0.75 wt.% MWCNT addition, suggests that the surface area of MWCNT exposed to polymer chains is not further increased because a trend of carbon nanotubes to bundle forming larger agglomerates, resulting in a reduction of the efficiency of nanotubes as confining surfaces.

Table 1 summarizes the thermal properties of composites obtained by DSC. It is worth to note that the lowering of the T_{cc} (cold crystallization peak temperature) from 119.9 °C for neat PLLA to 97–104 °C for its MWCNT composites is accompanied by an enlargement of cold crystallization temperature with respect to neat PLLA. The onset of cold crystallization at lower temperature in presence of MWCNT is interpreted in terms of the already reported nucleating agent effect of carbon nanotubes on polymer crystallization [43–45]. However, the overall cold crystallization determined by the exothermal enthalpy measured during the DSC in PLLA and its MWCNT composites is almost the same, unlike what was observed in a previous work with PLLA/SWCNT composites [46]. In the latter the presence of single wall carbon nanotubes not only changed the overall crystallinity of PLLA but also all parameters of its crystallization kinetics.

The nucleating effect of carbon nanotubes into PLLA is not very pronounced since when quenching a polymer from the melt to temperatures bellow T_g polymer chains have not enough time to reorganize themselves into a more ordered state, resulting in a predominantly amorphous structure. However, the crystalline fraction is increased by the presence of MWCNT contents up to 1.25 wt.%, giving raise to a 12.8% crystallinity degree. Further increase of nanotube concentration results in aggregation of adjacent nanotubes, giving rise to MWCNT bundles above the critical concentration of 1.25 wt.%. This effect yields a reduction of crystallinity together with cold crystallization temperature increase due to the reduction of nucleation surfaces provided by nanotubes. Hence, the existence of a critical concentration of MWCNT is demonstrated as previously observed for PLLA/SWCNT system [46].

Table 1
The respective average and standard deviation values of the studied thermal properties of PLLA/MWCNT composites determined by DSC.

% CNT	T_g (°C)	T_{cc} (°C)	ΔH_{cc} (J/g)	T_m (°C)	ΔH_m (J/g)	X_c (%)
0	56.6	119.9 ± 0.6	36.4 ± 2.1	169.3 ± 0.3	39.6 ± 1.1	3.1
0.75	61.9	102.8 ± 0.8	29.9 ± 0.4	169.4 ± 0.2	39.3 ± 0.5	8.9
1.25	61.6	97.4 ± 1.6	25.3 ± 0.8	169.5 ± 0.1	38.7 ± 1.4	12.8
2.5	62.1	100.5 ± 0.2	29.7 ± 2.2	169.5 ± 1.7	39.6 ± 2.1	9.6
4	61.4	102.5 ± 1.7	31.6 ± 2.3	169.2 ± 1.1	41.6 ± 2.1	9.8
5	61.7	104.6 ± 0.1	28.9 ± 0.4	169.3 ± 0,3	37.1 ± 0.3	8.2

3.2. Heat capacity measurements

The evolution of Specific Heat Capacities as a function of the MWCNT content in PLLA composites in the temperature range of −10 °C–20 °C (corresponding all of them to temperatures bellow T_g) is shown in Fig. 2.

Data scatter showed is due to the small differences in the arrangement of nanotubes into samples with the same composition. Three separated regions can be differentiated in function of carbon nanotube concentration of composites. For concentrations below 0.75 wt.% nanotubes act as efficient heat transfer elements through the composite and a decrease on heat capacity is achieved following the initially expected lowering trend. The specific heat capacity at 20 °C (see Table 2) decreases from a value of 1.007 J/g °C in neat PLLA to a minimum of 0.748 J/g °C in its 0.75 wt.% MWCNT composite counterpart. Then, C_p is smoothly recovered to attain approximately the value of neat PLLA for 1.5 wt.% MWCNT content. Finally, larger amounts of MWCNT yield increasing values ranging from 1.294 J/g °C to 1.487 J/g °C for the 2.5 and 5 wt.% MWCNT compositions respectively. It is worth noting that the C_p value for 5 wt.% composite exceeds that of neat PLLA in a 47%. This could be viewed in a first instance as a surprising result since the specific heat capacity of carbon nanotubes at 293 K is in the range of 0.60–0.68 J/g °C [47–49]; which is quite lower than that of the neat PLLA.

The disparity between predicted and obtained values and the presence of a critical concentration at 0.75 wt.% in which the C_p of nanotubes do not contribute to reducing the heat capacity of the composites can be associated with the altered heat transfer mechanism within the composites induced by the polymer–nanotube and nanotube–nanotube interfaces. In addition, the aggregation of

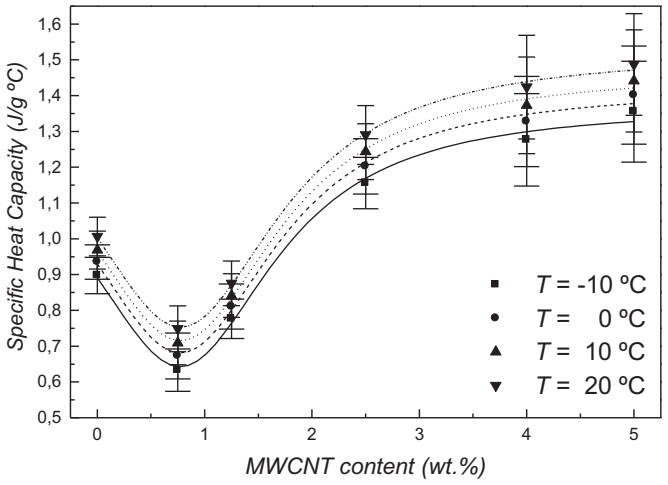

Fig. 2. Evolution of the average and standard deviation specific heat capacity of PLLA/MWCNT composites depending on the carbon nanotube concentration at different temperatures.

Table 2
The respective average and standard deviation specific heat capacity values of PLLA/MWCNT composites at 20 °C.

% MWCNT	Specific heat capacity, J/g °C
0	1.007 ± 0.054
0.75	0.748 ± 0.064
1.25	0.877 ± 0.062
2.5	1.294 ± 0.082
4	1.424 ± 0.145
5	1.487 ± 0.142

carbon nanotubes creates a graphitic effect, with interactions between tubes dampening the 1D nature of the CNT [50]. Thus, larger amount of aggregation changes the heat capacity behaviour of carbon nanotubes, resulting in a composite with higher specific heat capacity at concentrations above 1.25 wt.%. It deserves to be noted that this *Specific heat capacity* enhancement induced by the MWCNT addition occurs when nanotubes are inefficiently dispersed within the polymer matrix.

3.3. Thermal conductivity estimation

The heat transfer in carbon nanotubes may be correlated to a phonon-conduction mechanism. In this paper, we try to understand the thermal-conduction mechanisms involved within polymer/CNT nanocomposites. In this way, thermal conductivity at room temperature has been worked out through the constitutive relation:

$$K = D\rho c_p \tag{5}$$

where D is the thermal diffusivity (mm^2/s), ρ is bulk density (g/cm^3) and C_p is specific heat capacity (J/g °C). The error in thermal conductivity has been estimated by means of error theory as follows:

$$\Delta K = \Delta D\rho C_p + D\Delta\rho C_p + D\rho\Delta C_p \tag{6}$$

For this reason, thermal diffusivity and the density of PLLA/MWCNT composites were measured.

Thermal diffusivity values of composites in function of carbon nanotube concentration are represented in Fig. 3. As expected from the large thermal diffusivity of nanotubes comparing with that of neat PLLA [51–53], an increasing general trend in thermal diffusivity with the addition of carbon nanotubes is observed. The evolution of thermal diffusivity with MWCNT content presents a similar behaviour as for the specific heat capacity; with three regions depending on the nanotube loading. After the initial drop in diffusivity for concentrations up to 1.25 wt.% MWCNT, a rapid increase in D is achieved until 2.5 wt.%. This behaviour might be due to the existence of a polymer–nanotube interfacial thermal resistance as will be shown later in Fig. 4. Further addition of nanotubes results in a linear increment of thermal diffusivity, reaching an increase of 39% for 5 wt.% composite. This increase may be due to the development of a more extensive conductive network as will be discussed later.

The theoretical density of PLLA/MWCNT composites was calculated as follows:

$$\rho = \frac{1}{\frac{\omega_{PLLA}}{\rho_{PLLA}} + \frac{\omega_{MWCNT}}{\rho_{MWCNT}}} \tag{7}$$

where ω_{PLLA} and ω_{MWCNT} are the weight fractions of PLLA and carbon nanotubes respectively and ρ_{PLLA} and ρ_{MWCNT} are the densities of row PLLA set at 1.2484 g/cm^3 (for a crystallinity degree of 8.77% of the α-form, taking into account the densities of 1.245 g/cm^3 for amorphous PLLA and 1.285 g/cm^3 for fully crystalline PLLA [54]) and the as-received MWCNT (2.0 g/cm^3) respectively. Composite densities were measured by means of gas displacement technique in a nitrogen atmosphere (Micrometrics AccuPyc II 1340 Pycnometer) at 23 ± 1 °C. Table 3 reports the average values over four samples of measured densities.

Once thermal diffusivity, bulk density and specific heat capacity of composites were obtained, the determination of the thermal conductivity was carried out by means of Eq. (5). Fig. 4 shows the estimation of thermal conductivity as a function of MWCNT volume concentration (calculated from the weight fraction of both components and their densities).

As can be seen, the thermal conductivity of neat PLLA is found to be 0.165 W/m K, which falls in the typical range for polymers (0.1–0.2 W/m K). The addition of carbon nanotubes yields a large enhancement of thermal conductivity, with increased conductivities of about 100% for a volume fraction of 3%.

As stated above in Figs. 2 and 3 for *specific heat capacity* and *diffusivity* of composites, thermal conductivity also shows three separated regions as a function of MWCNT. As can be seen, thermal

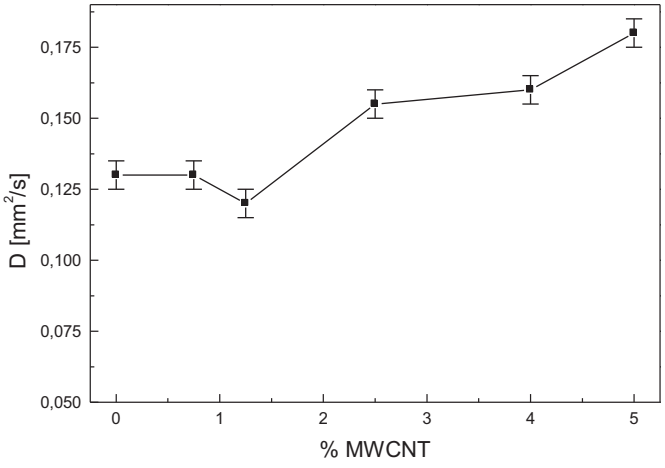

Fig. 3. Thermal diffusivity values of composites as a function on MWCNT concentration. Deviation corresponds to the resolution of the experimental technique.

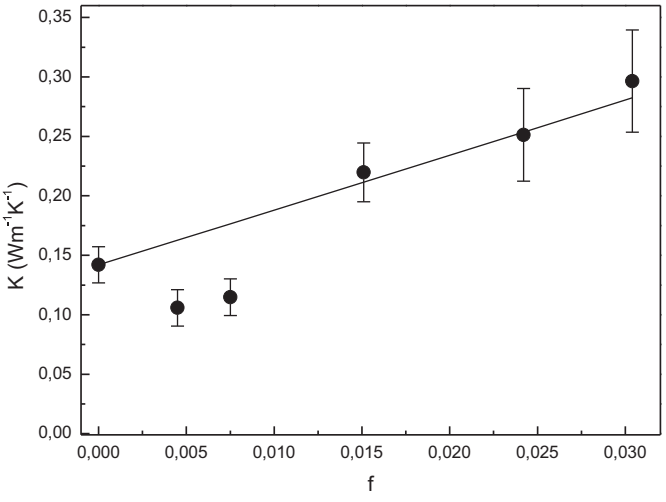

Fig. 4. Thermal conductivity of the PLLA/MWNT composite as a function of the volume fraction. Dots are the experimental results and the line shows the fitting to Eq. (8).

Table 3
Theoretical (from Eq. (7)) and experimental densities (both respective average and standard deviation values) of PLLA/MWCNT composites.

W_f (%)	V_f (%)	$\rho_{theo.}$ (g/cm^3)	$\rho_{meas.}$ (g/cm^3)
0	0	1.2484	1.2517 ± 0.0015
0.75	0.45	1.2519	1.2523 ± 0.0024
1.25	0.75	1.2543	1.2546 ± 0.0018
2.5	1.51	1.2602	1.2611 ± 0.0028
4	2.42	1.2675	1.2714 ± 0.0022
5	3.04	1.2723	1.2752 ± 0.0037

conductivity drops by 14% with the addition of 0.45 vol.% of nanotubes. This deviation from the theoretical prediction carried out by Eq. (8) (see the line in Fig. 4) could seem counterintuitive since the much larger thermal conductivity of carbon nanotubes compared with neat PLLA. However, this reduction can be explained in terms of the presence of an interfacial resistance between the nanotubes and the matrix in which phonon scattering reduces the bulk thermal conductivity. As will be shown in Fig. 7, the arrangement of nanotubes within the polymer matrix also affects the thermal conductivity since at low concentrations the nanotubes are separately dispersed and they do not contribute to the conductive pathway, providing thermal insulator properties to the composite. After reaching a critical concentration, thermal conductivity increases with the addition of nanotubes. The presence of a critical carbon nanotube concentration in which a shift in the thermal conductivity trend occurs has been previously reported by several authors [23,55]. It is remarkable that despite the achieved enhancement on the thermal conductivity is not as high as expected due to the interfacial thermal resistance effects, the increase of 100% on the thermal conductivity at 3 vol.% is larger than that obtained for other polymer/carbon nanotube composites such as PEEK/MWCNT [22] (133% at 17 wt.% loading), PVC/MWCNT [23] (1% at 0.7 vol.%), PMMA/SWCNT [24] (150% at 9 vol.%) or PVDF/SWCNT [25] (19% at 5 wt.%).

The theoretical framework known as Effective Medium Approach (EMA) describes the effective thermal conductivity in the case of nanotube composites with randomly oriented nanotubes at low concentrations. The model developed by Nan et al. [31] takes into account the thermal conductivity values of both matrix and nanotubes, the dimensions of the individual rods, as well as the interfacial resistance at the nanotubes/matrix interface. The effective thermal conductivity, K_e, reads

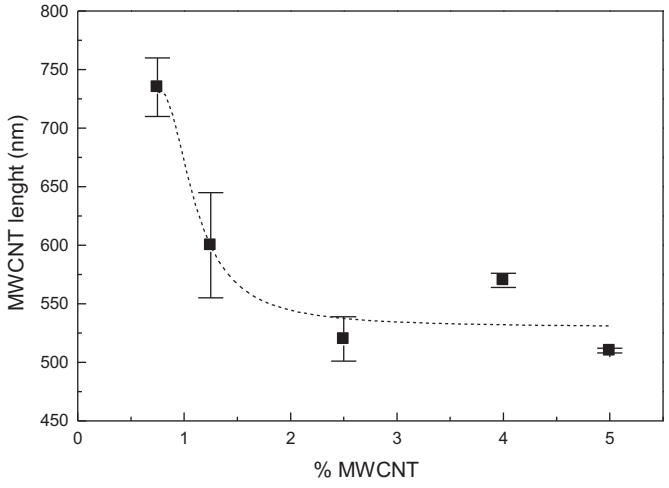

Fig. 5. Carbon nanotube extrapolated average and standard deviation length values depending on MWCNT concentration.

$$K_e = K_m\left(\frac{3+f(\beta_x+\beta_z)}{3-f\beta_x}\right) \tag{8}$$

where K_m is the matrix thermal conductivity (measured in this work to be 0.165 W m^{-1} K^{-1}), f is the volume fraction of the nanotubes.

$$\beta_x = \frac{2(K_{11}^c - K_m)}{K_{11}^c + K_m} \quad \beta_z = \frac{K_{33}^c}{K_m} - 1 \tag{9}$$

K_{11}^c and K_{33}^c are the equivalent thermal conductivities along transverse and longitudinal axes of an individual nanotube coated with a very thin interfacial thermal-barrier layer

$$K_{11}^c = \frac{K_c}{1+\frac{2a_k}{d}\frac{K_c}{K_m}} \quad K_{33}^c = \frac{K_c}{1+\frac{2a_k}{L}\frac{K_c}{K_m}} \tag{10}$$

where the Kapitza radius a_k is defined by $a_k = R_k K_m$ and R_k is the interfacial resistance at the interface. K_c is the thermal conductivity of an individual nanotube. Published experimental measurements [13,14] place this value in a range between 1750 and 3000 W m^{-1} K^{-1}, while a simulated one gives 6600 W m^{-1} K^{-1} [15].

The estimation of the nanotube length for the calculation of the effective medium approach (EMA) was done by means of dynamic light scattering (DLS). Fig. 5 shows the extrapolated nanotube length depending on the MWCNT concentration. Those values were obtained by measuring fine-black suspensions of all the compositions after bath ultrasonication for different times and extrapolating those values to $t = 0$ min. The nanotube lengths are comprised in a range between 510 and 735 nm, which is notably smaller than the length of 0.1–10 μm reported by the supplier. During the melt mixing of composites, the mechanical forces such as pressing forces, shearing forces and rubbing forces induced by the two rotors can directly cut the carbon nanotubes. Moreover, during this process molten PLLA acts as a soft cutting medium resulting in even an increased shortening effect of nanotubes [56]. It can be noted that an increase in nanotube concentration results in shorter MWCNT together with a more uniform length distribution (the standard length deviation is continuously reduced from 45 nm for the 1.25 wt.% composite to 2 nm for the 5 wt.% composite respectively). Mixing composites with larger amounts of nanotubes leads to an increased viscosity of composites which results in stronger shearing forces when mixing and hence shorter nanotubes and narrower length distributions are achieved [57]. A critical length of about 520–540 nm below which the nanotube length cannot be further reduced is found. So, according to DLS measurements and TEM micrographs (as shown in Fig. 7), in the present work, the average diameter of the nanotubes was set to $d = 10$ nm, while the length was $L = 590 \pm 90$ nm (Eq. (10)).

It is worth to note that the considerable reduction in CNT length during melt mixing reduced the large aspect ratio of nanotubes, resulting in less effective reinforcing elements for polymer nanocomposites. Indeed, this reduction of 30% on the nanotube length with the addition of 5 wt.% would lead to larger electrical percolation thresholds (the electrically conductive three-dimensional network is achieved at higher loadings) [58] and lower thermal conductivities for a given concentration (CNT length reduction carries as well a reduction of the free length of path). Thus, it is suggested that nanotube length reduction during the mixing process is an important issue that has to be overcome in order to obtain an increased performance of carbon nanotube-based polymer composites.

A value of $K_c = 3000$ W m^{-1} K^{-1} was used for the fitting and a good agreement was found for the thermal conductivity enhancement between the model and the experimental values for a thermal interface resistance of $R_k = (1.8 \pm 0.3) \times 10^{-8}$ m^2 K/W. R_k results are in

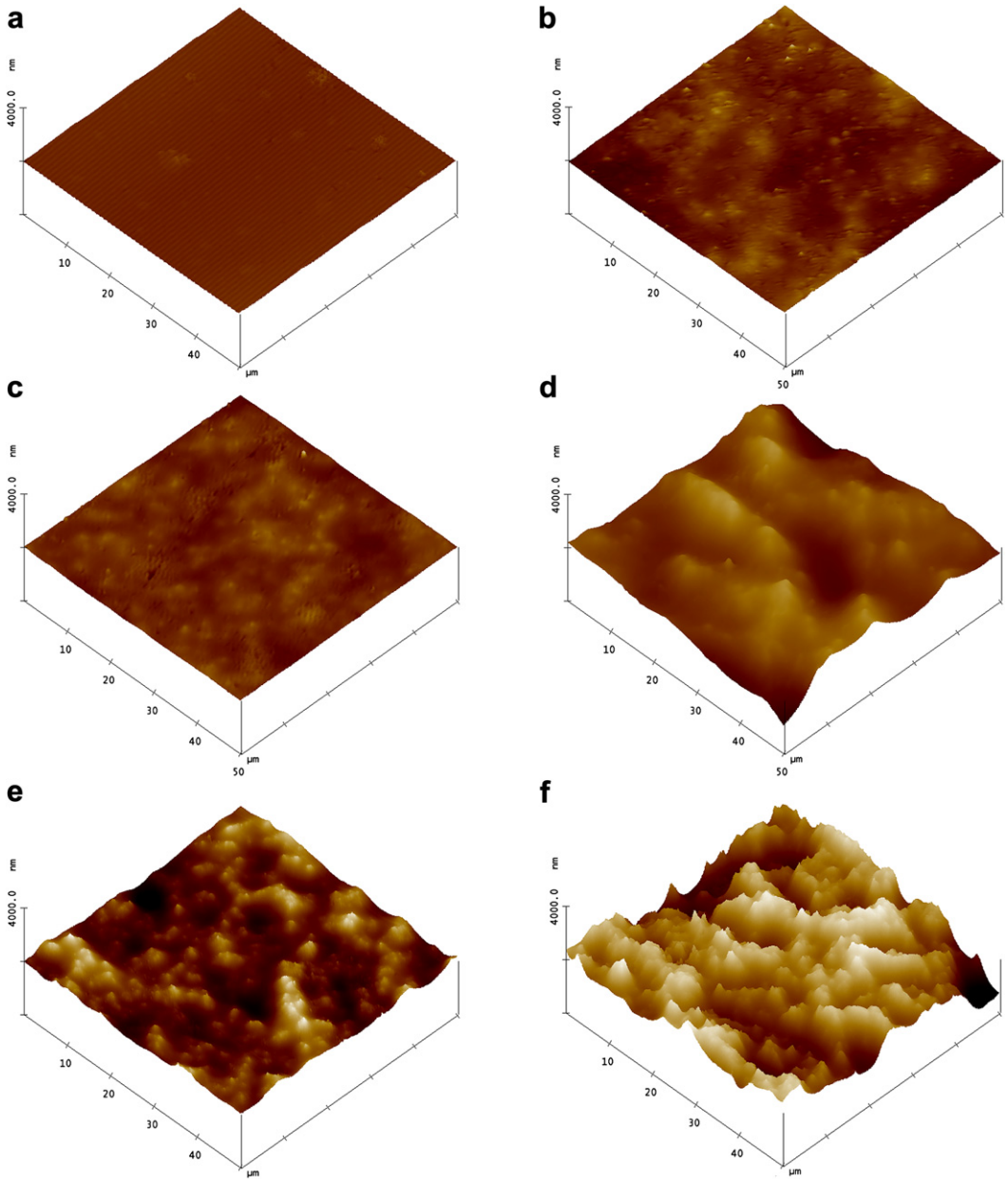

Fig. 6. Contact-mode 3D AFM images showing carbon nanotube dispersion within the PLLA matrix at different MWCNT concentration. (a) 0 wt.%; (b) 0.75 wt.%; (c) 1.25 wt.%; (d) 2.5 wt.%; (e) 4 wt.%; (f) 5 wt.%. XY scales are 50 μm. All height scales are 4000 nm.

their turn in agreement with the values found in literature for other nanotube composites, either experimentally [59,60] or through Monte Carlo simulations [61]. The fitted results are shown in Fig. 5.

There are simpler models for the effective thermal conductivity which do not take into account neither the thermal resistance interface, nor the dimensions of the nanotubes [31] but, in order to fit the results to them, it would be needed to consider an unrealistic low value of the thermal conductivity of a single nanotube, of about 10–15 W m^{-1} K^{-1}. This result assesses the importance of using physically sensible models to interpret the thermal conductivity of these systems, stressing the role of the interfacial thermal resistance between the matrix and the nanotubes.

3.4. Microstructural features

It is well known that the obtained morphology influences the biodegradability as well as the physico-mechanical properties of resulting PLLA, conditioning the potential uses for biomedical and packaging applications [62]. The atomic force microscopy (AFM) is a very resourceful tool for determining the surface topology of materials giving access to 3D morphology details [63]. Since good dispersion of carbon nanotubes into polymer matrix is essential from the aspect of specific heat capacity, thermal conductivity and thermal diffusivity, AFM studies at room temperature were conducted to analyze the uniformity of dispersions of the filler as well as for characterize the surface morphology and roughness of PLLA/MWCNT composites.

Fig. 6 shows the representative AFM 3D surface topology of the samples containing 0, 0.75, 1.25, 2.5, 4 and 5 wt.% MWCNT. For the seek of comparison in those images all *Z* vertical scales were maintained at 4000 nm. It is worth to note that topology features are dependant on the carbon nanotube concentration. Increasing carbon nanotube concentration surface becomes much rougher, containing larger surface irregularities. Surface remains almost flat

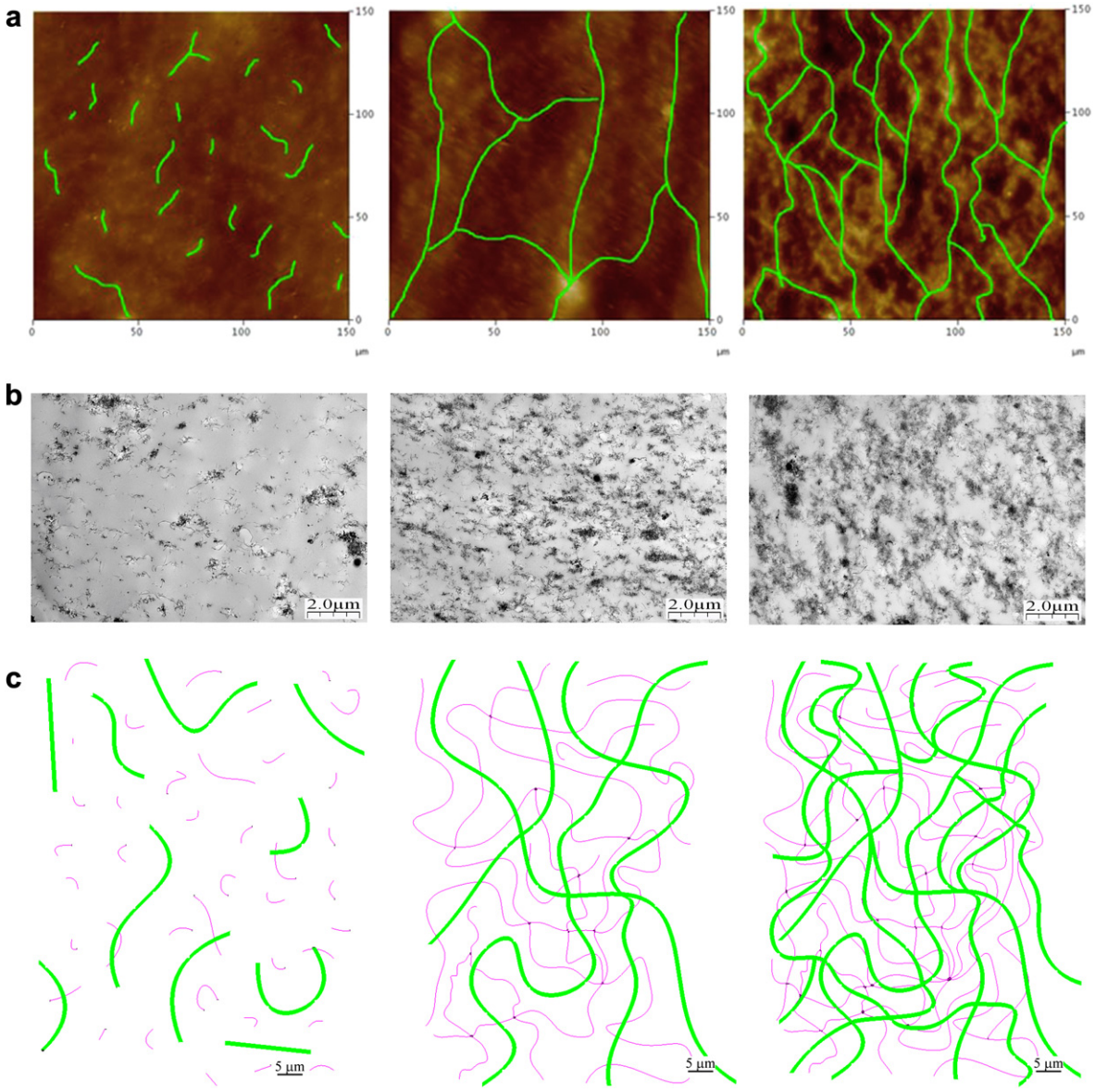

Fig. 7. Conducting pathway for PLLA/MWCNT composites at different concentrations; (left) 0.75 wt.%; (middle) 2.5 wt.% and (right) 5 wt.%. (a) AFM images; (b) TEM micrographs at 11,500×; (c) Schematical representation showing macro-scale (green lines) and micro-scale conducting pathways (pink lines). (For interpretation of the references to colour in this figure legend, the reader is referred to the web version of this article.)

with the addition of nanotubes up to 1.25 wt.%. At higher loadings MWCNT yields a "*mountain-valley*" feature at micrometer scale whose valley's depth ranges from 72 nm for composite containing 1.25 wt.% to 953 nm for its 5 wt.% composite, resulting in a sixfold rougher surface. As MWCNT content increases some aggregates appear at top surface, providing more irregular shape and rougher surfaces in regard to that found in neat polymer.

Table 4 summarizes the quantitative average values over 5 samples of surface roughness parameters of PLLA/MWCNT composites obtained by AFM. The report of those parameters as a function of reinforcement concentration allows one to directly differentiate the effect of carbon nanotubes on PLLA surface morphology. Results reveal that increasing nanotube loading R_q and R_a parameters increased notably; indicating that surface becomes much rougher. The density of the homogenously distributed aggregates increases from 8000 to 31,200 mm^{-2} as carbon nanotube concentration increases from 0.75 to 5 wt.%. In addition, the diameter of those nanotube aggregates, as confirmed by AFM images evolve from 4 μm (at 0.75 wt.%) to 14 μm (5 wt.%). As can be seen, there is no preferential orientation of aggregates, providing isotropic thermal properties to PLLA/MWCNT composites. Hence, AFM analysis reveals that lower degree of reinforcements leads to negligible amounts of aggregates, showing an almost flat topology. By means of adding nanotubes to the polymer, however, a larger

Table 4
Surface morphology parameters (both average and standard deviation values) of PLLA/MWCNT composites extracted from AFM images.

% CNT	Aggregate density ($1/mm^{-2}$)	Roughness parameters (nm)	
		R_a	R_q
0	0	10 ± 1	12 ± 2
0.75	8000 ± 445	19 ± 7	25 ± 9
1.25	10,400 ± 720	28 ± 2	35 ± 4
2.5	25,400 ± 1760	87 ± 15	111 ± 29
4	28,800 ± 2170	102 ± 13	134 ± 21
5	31,200 ± 2620	175 ± 19	220 ± 34

amount of aggregation of MWCNT is found leading to additional irregularities of the PLLA/MWCNT composites, in which rougher surfaces are obtained. For instance, the surface roughness of PLLA/MWCNT 5 wt.% composite was increased by 18 times in regard to neat polymer.

Fig. 7 shows the carbon nanotube dispersion within the PLLA by AFM images (Fig. 7a) and TEM micrographs (Fig. 7b) of the samples containing 0.75, 2.5 and 5 wt.% MWCNT. For all the concentrations nanotube aggregates appears randomly distributed over the entire matrix, with no preferential orientation. Due to the crystalline graphite structure of nanotubes (they present higher free length of path and higher number of phonon vibration modes as compared with neat polymer) the phonon transport within the composites occurs preferably through the CNT network.

At low concentrations, 0.75 wt.% MWCNT for example, nanotubes are observed as separated individual tubes and they do not contribute to the conductive pathway, providing thermal insulator properties to the composite. In this region the interfacial thermal resistance is enough to dismiss the bulk thermal conductivity of composites. On the contrary, at concentrations larger than 1.25 wt.%, nanotubes are forming an interconnected structure, providing a thermally conducting pathway which increases the thermal phonon conduction. In this region the formation of conducting network is enough to counteract the thermal boundary resistance and the bulk thermal conductivity is increased in regard to neat polymer, enhancing the efficiency of nanotubes as thermal conductors in PLLA. Further addition of nanotubes results in higher density of conductive network with more numerous conduction pathways, facilitating the phonon transport through the network and yielding an increased overall thermal conductivity. Moreover, larger CNT concentrations result in a reduced distance between percolated nanotubes, which enables easier phonon conduction by reduced phonon scattering. These morphological features are in good agreement with thermal conductivity values reported on Fig. 5, which shows a dual effect of nanotubes on the thermal conductivity of the resulting composite.

A schematical representation of the development of the thermally conductive pathways with the addition of carbon nanotubes accomplished by the development of a macro-scale heat conducting pathways (green lines) formed by CNT aggregates and by the development of a micro-scale heat conducting pathways (pink lines) formed by individual carbon nanotubes is shown in Fig. 7c. The formation of those conducting pathways for concentrations larger than 1.25 wt.% MWCNT enables a higher free length of path within the nanocomposite, in which the transport of thermal energy occurs by phonon-conduction mechanism, enhancing the efficiency of nanotubes as thermal conductors within PLLA.

Due to the large heat resistance between one nanotube to another nanotube, better dispersion of nanotubes within polymer matrix would result in a reduction of direct coupling between nanotubes, reducing the intense phonon scattering and yielding an enhancement on the thermal conductivity of composite [64] for a given MWCNT concentration.

4. Conclusion

In this work the thermal properties of PLLA/MWCNT composites were investigated as a function of MWCNT concentration. Specific heat capacity, thermal diffusivity and thermal conductivity results reveal a twofold effect of MWCNT on PLLA heat transfer process. At concentrations up to 0.75 wt.%, carbon nanotubes reduce the *specific heat capacity* of composites by 26%. Larger concentrations result in larger values of C_p up to 1.487 J/g °C for the 5 wt.% composite, because of the aggregation effect of nanotubes which are dampening the 1D nature of the CNT. Thermal diffusivity shows similar trend of the specific heat capacity. A remarkable enhancement of 100% on the thermal conductivity with a carbon nanotube volume fraction of 3 vol.% was obtained. At concentrations up to 0.75 wt.% thermal conductivity is reduced with the addition of carbon nanotubes due to the presence of an interfacial resistance in which phonon scattering reduces the bulk thermal conductivity. With further addition of CNT a network of higher density of conducting pathways is achieved and the resulting thermal conductivity increases. The large polymer-CNT thermal interface resistance in which a strong phonon scattering occurs reduces the theoretically predicted thermal conductivity of composite. In this way, with the aid of the theoretical framework provided by the effective medium approach (EMA) the thermal interface resistance was found to be $R_k = (1.8 \pm 0.3) \times 10^{-8}$ m^2 K/W. AFM images and TEM micrographs reveal the formation of a thermally conducting pathway for concentrations larger or equal than 2.5 wt.% MWCNT. At low nanotube concentrations thermal interface resistance is enough to dismiss the bulk thermal conductivity of composite. On the contrary, at concentrations equal or higher than 2.5 wt.%, nanotubes form an interconnected structure, providing a conducting pathway for thermal transport. In this region the formation of conducting network is enough to counteract the thermal boundary resistance and the bulk thermal conductivity is increased in regard to neat polymer.

In this paper we have explore the possibilities of an important increase of the thermal conductivity as compared to the electrical percolation phenomena well known in these materials. Although the reduction of thermal interface resistance and the improvement of nanotube dispersion within polymer matrix will be necessary for further applications, those results indicate that carbon nanotubes can be effectively use for enhancing of thermal conductivity of PLLA. The next important step towards the complete understanding of thermal-conduction mechanism will be the measurement of thermal conductivity at low temperatures and in this way separate the contribution of electron conduction to the heat transport in CNT-based polymer nanocomposites. In addition, electrical and thermal conductivities will be correlated in the future to obtain further information on the thermal-conduction mechanism in polymer/CNT composites.

Acknowledgements

The authors are thankful for funds of the European Community (POCO project, 7th FP, NMP-213939) and of the Basque Government, Department of Education, Universities and Research (GIC10/152-IT-334-10, IT351-10), Department of Industry (IE 10/276) and University of the Basque Country (UFI11/55). E.L thanks the University of the Basque Country for a postdoctoral fellowship. SGIker (UPV/EHU) technical support for TEM measurements is also gratefully acknowledged.

References

[1] Iijima S. Nature 1991;354(6348):56–8.
[2] Iijima S. Physica B 2002;323(1–4):1–5.
[3] Sandler JKW, Kirk JE, Kinloch IA, Shaffer MSP, Windle AH. Polymer 2003;44(19):5893–9.
[4] Ounaies Z, Park C, Wise KE, Siochi EJ, Harrison JS. Composites Sci Technol 2003;63(11):1637–46.
[5] Meincke O, Kaempfer D, Weickmann H, Friedrich C, Vathauer M, Warth H. Polymer 2004;45(3):739–48.
[6] Mierczynska A, Mayne-L'Hermite M, Boiteux G, Jeszka JK. J Appl Polym Sci 2007;105(1):158–68.
[7] Lizundia E, Sarasua JR, D'Angelo F, Martino S, Orlacchio A, Kenny JM, et al. Macromol Biosci; 2012. doi:10.1002/mabi.201200008.
[8] Bonnet P, Sireude D, Garnier B, Chauvet O. Appl Phys Lett 2007;91(20):201910–3.
[9] Kumar S, Alam MA, Murthy JY. Appl Phys Lett 2007;90:104105.

[10] Haggenmueller R, Guthy C, Lukes JR, Fischer JE, Winey KI. Macromolecules 2007;40(7):2417–21.
[11] Hone J, Batlogg B, Benes Z, Johnson AT, Fischer JE. Science 2000;289(5485):1730–3.
[12] Hone J, Llaguno MC, Biercuk MJ, Johnson AT, Batlogg B, Benes Z, et al. Appl Phys A-Mater Sci Process 2002;74(3):339–43.
[13] Biercuk MJ, Llaguno MC, Radosavljevic M, Hyun JK, Johnson AT, Fischer JE. Appl Phys Lett 2002;80(15):2767–9.
[14] Kim P, Shi L, Majumdar A, McEuen PL. Phys Rev Lett 2001;87(21):215502/1–215502/4.
[15] Berber S, Kwon Y, Tomanek D. Phys Rev Lett 2000;84(20):4613–6.
[16] Cai D, Song M. Carbon 2008;46(15):2107–12.
[17] Koo J, Kang Y, Kleinstreuer C. Nanotechnology 2008;19:375705-1–375705-7.
[18] Landi BJ, Raffaelle RP, Heben MJ, Alleman JL, Van Derveer W, Gennett T. Nano Lett 2002;2(11):1329–32.
[19] Roberts JA, Imholt T, Ye Z, Dyke CA, Price DW, Tour JM. J Appl Phys 2004;95(8):4352–6.
[20] Rahman GMA, Guldi DM, Cagnoli R, Mucci A, Schenetti L, Vaccari L, et al. J Am Chem Soc 2005;127(28):10051–7.
[21] King JA, Tucker KW, Vogt BD, Weber EH, Quan C. Polym Composites 1999;20(5):643–54.
[22] Bangarusampath DS, Ruckdäschel H, Altstädt V, Sandler JKW, Garray D, Shaffer MSP. Polymer 2009;50(24):5803–11.
[23] Mamunya Y, Boudenne A, Lebovka N, Ibos L, Candau Y, Lisunova M. Composites Sci Technol 2008;68(9):1981–8.
[24] Guthy C, Du F, Brand S, Winey KI, Fischer JE. J Heat Transf Trans ASME 2007;129(8):1096–9.
[25] Xu Y, Ray G, Abdel-Magid B. Composites Part A: Appl Sci Manufacturing 2006;37(1):114–21.
[26] Kapitza PL. Collected papers of P.L. Kapitza 1965;2:581.
[27] Every AG, Tzou Y, Hasselman DPH, Raj R. Acta Metallurgica et Materialia 1992;40(1):123–9.
[28] Swartz ET, Pohl RO. Rev Mod Phys 1989;61(3):605–68.
[29] Shenogin S, Xue L, Ozisk R, Keblinski P. J Appl Phys 2004;95(12):8136–44.
[30] Prasher R. Phys Rev B 2008;77(7):075424.
[31] Nan C-, Shi Z, Lin Y. Chem Phys Lett 2003;375(5–6):666–9.
[32] Nan C, Liu G, Lin Y, Li M. Appl Phys Lett 2004;85(16):3549–51.
[33] Martina M, Hutmacher DW. Polym Int 2007;56(2):145–57.
[34] Auras R, Harte B, Selke S. Macromol Biosci 2004;4(9):835–64.
[35] Pan P, Zhu B, Inoue Y. Macromolecules 2007;40:9664–71.
[36] Gross RA, Kalra B. Science 2002;297(5582):803–7.
[37] Lee W, Parpura V. Nanoneurosci Nanoneuropharmacol 2009;180:111–25.
[38] Gibson RF. Compos Struct 2010;92(12):2793–810.
[39] Arkema. 2008.
[40] Sarasua JR, Pru'homme RE, Wisniewski M, Le Borgne A, Spassky N. Macromolecules 1998;31:3895–905.
[41] del Rio J, Etxeberria A, López-Rodriguez N, Lizundia E, Sarasua JR. Macromolecules 2010;43:4698–707.
[42] Chirtoc M, Dadarlat D, Bicanic D, Antoniow JS, Egée M. Prog Photothermal Photoacoustic Sci Technol 1997;3:185–251.
[43] Wiemann K, Kaminsky W, Gojny FH, Schulte K. Macromol Chem Phys 2005;206(15):1472–8.
[44] Lu K, Grossiord N, Koning CE, Miltner HE, van Mele B, Loos J. Macromolecules 2008;41(21):8081–5.
[45] Coleman JN, Cadek M, Ryan KP, Fonseca A, Nagy JB, Blau WJ, et al. Polymer 2006;47(26):8556–61.
[46] Lizundia E, Landa P, Gonzalez JJ, Sarasua JR. ANTEC Proc; 2009:2517–20.
[47] Zhang S, Xia M, Zhao S, Xu T, Zhang E. Phys Rev B 2003;68(7):075415/1–075415/7.
[48] Dobardzic E, Milosevic I, Nikolic B, Vukovic T, Damnjanovic M. Phys Rev B 2003;68(4):045408/1–045408/9.
[49] Wu MCH, Hsu J. Nanotechnology 2009;20(14):145401.
[50] Benedict LX, Louie SG, Cohen ML. Solid State Commun 1996;100(3):177–80.
[51] Borca-Tasciuc T, Vafaei S, Borca-Tasciuc DA, Wei BQ, Vajtai R, Ajayan PM. J Appl Phys 2005;98(5):054309.
[52] Hou J, Wang X, Liu C, Cheng H. Appl Phys Lett 2006;88(18):181910.
[53] Xie H, Cai A, Wang X. Phys Lett A 2007;369(1–2):120–3.
[54] Sawai D, Tsugane Y, Tamada M, Kanamoto T, Sungil M, Hyon S. J Polym Sci Part B: Polym Phys 2007;45(18):2632–9.
[55] Grunlan JC, Kim Y, Ziaee S, Wei X, Abdel-Magid B, Tao K. Macromol Mater Eng 2006;291(9):1035–43.
[56] Chen L, Pang X, Yu Z. Mater Sci Eng A 2007;457(1–2):287–91.
[57] Chen L, Pang X, Zhang Q, Yu Z. Mater Lett 2006;60(2):241–4.
[58] Bauhofer W, Kovacs JZ. Composites Sci Technol 2009;69(10):1486–98.
[59] Bryning MB, Milkie DE, Islam MF, Kikkawa JM, Yodh AG. Appl Phys Lett 2005;87(16):161909/1–161909/3.
[60] Gao L, Zhou X, Ding Y. Chem Phys Lett 2007;434(4–6):297–300.
[61] Foygel M, Morris RD, Anez D, French S, Sobolev VL. Phys Rev B: Condensed Matter Mater Phys 2005;71(10):104201/1–104201/8.
[62] Sarasua JR, Arraiza AL, Balerdi P, Maiza I. Polym Eng Sci 2005;45(5):745–53.
[63] Lizundia E, Landa P, Sarasua JR. ANTEC Proc; 2011:230–5.
[64] Maruyama S, Igarashi Y, Taniguchi Y, Shiomi J. J Therm Sci Technol 2006;1(2):138–48.